Chinese Chemical Letters 33 (2022) 1065–1069

Contents lists available at ScienceDirect

Chinese Chemical Letters

journal homepage: www.elsevier.com/locate/cclet

Enhanced catalytic activity of Ru through N modification toward alkaline hydrogen electrocatalysis

Yuanmeng Zhao[a,1], Xuewei Wang[a,1], Zhen Li[a,1], Pingping Zhao[b,**], Congliang Tao[c], Gongzhen Cheng[a], Wei Luo[a,d,e,*]

[a] College of Chemistry and Molecular Sciences, Wuhan University, Wuhan 430072, China
[b] School of Printing and Packaging, Wuhan University, Wuhan 430072, China
[c] Wuhan Foreign Language School, Wuhan 430022, China
[d] Suzhou Institute of Wuhan University, Suzhou 215123, China
[e] Yangzhou Kairuite Medical Products Co., Ltd., Yangzhou 225200, China

ARTICLE INFO

Article history:
Received 28 April 2021
Revised 16 May 2021
Accepted 18 May 2021
Available online 25 May 2021

Keywords:
Hydrogen oxidation reaction
Hydrogen evolution reaction
Ru
N-incorporation
DFT

ABSTRACT

Exploring highly efficient electrocatalysts and understanding the reaction mechanisms for hydrogen electrocatalysis, including hydrogen oxidation reaction (HOR) and hydrogen evolution reaction (HER) in alkaline media are conducive to the conversion of hydrogen energy. Herein, we reported a new strategy to boost the HER/HOR performances of ruthenium (Ru) nanoparticles through nitrogen (N) modification. The obtained N-Ru/C exhibit remarkable catalytic performance, with normalized HOR exchange current density and mass activity of 0.56 mA/cm^2 and 0.54 mA/μg, respectively, about 4 and 4.5 times higher than those of Ru/C, and even twofold enhancement compared to commercial Pt/C. Moreover, at the overpotential of 50 mV, the normalized HER current density of N-Ru/C is 5.5 times higher than that of Ru/C. Experimental and density functional theory (DFT) results verify the electronic regulation of Ru after N incorporation, resulting in the optimized hydrogen adsorption Gibbs free energy (ΔG_{H^*}) and hence enhancing the HOR/HER performance.

Hydrogen has been regarded as an effective energy carrier to replace traditional fossil energy for sustainable development in the future in terms of its significant advantage of zero emission and high gravimetric energy density [1-4]. Hydrogen oxidation reaction (HOR) in fuel cells and hydrogen evolution reaction (HER) in water electrolyzers are two crucial reactions during the hydrogen cycle [5,6]. Currently, the development of anion-exchange membranes (AEMs) permits the use of low-cost and earth-abundant platinum-free catalysts to meet the requirements toward oxygen reduction reaction (ORR) and oxygen evolution reaction (OER) [7-9]. Thus, the corresponding AEM-based fuel cells (AEMFCs) and water electrolysers in alkaline media have received considerable attention. However, even for the state-of-the-art Pt-based catalysts, their HOR/HER kinetics are approximately two to three orders of magnitude slower in alkali electrolytes than those in acidic electrolytes [10,11]. Therefore, exploring highly efficient Pt-free electrocatalysts combining with their catalytic mechanisms toward HOR/HER in alkaline media is highly desirable but still remains a challenge.

Recently, Ru and Ru-based materials have received great interests due to the potential to replace Pt-based electrocatalysts for catalyzing HOR/HER [12-21]. However, most of their performances are still far inferior to those of commercial Pt. Regulation of electronic structure of catalysts is an important strategy to boost the catalytic performance [22,23]. Therefore, great efforts have been committed to tailoring the catalysts' electronic structures, including alloying [24–27], forming heterogeneous structures [28-31] and lattice strain [32-34], *etc*. These methods always introduce additional variables, for example composition change. Heteroatom doping is a prospective approach that can modulate the electronic structure of host materials without changing their compositions by introducing charge redistribution [35-40]. Nevertheless, as far as we know, rationally adjusting the electronic structure of transition metals by the heteroatom doping method for facilitating alkaline HOR/HER performances has been rarely reported.

Herein, we reported the synthesis of N-incorporation Ru nanoparticles (N-Ru/C), and its remarkable catalytic performances

* Corresponding author at: College of Chemistry and Molecular Sciences, Wuhan University, Wuhan 430072, China.
** Corresponding author.
E-mail addresses: ppzhao@whu.edu.cn (P. Zhao), wluo@whu.edu.cn (W. Luo).
[1] These authors contributed equally to this work.

https://doi.org/10.1016/j.cclet.2021.05.038
1001-8417/

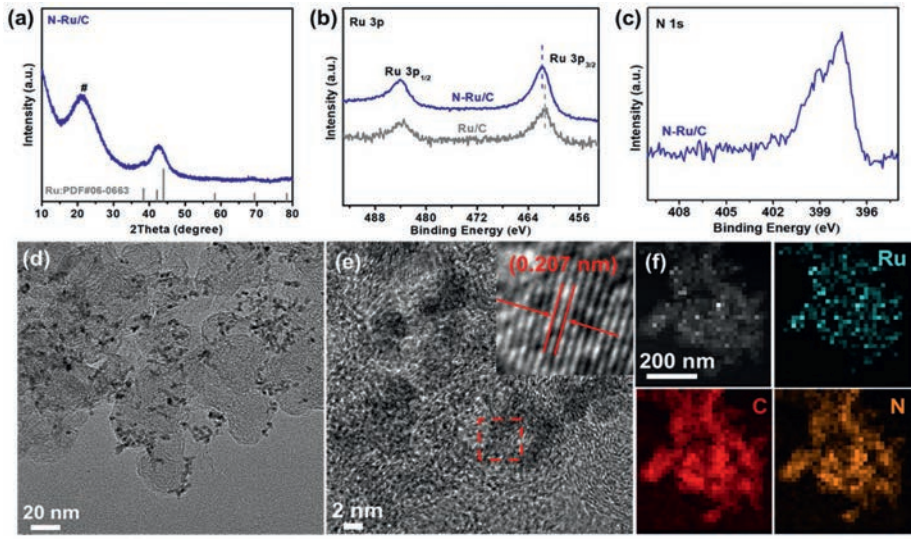

Fig. 1. (a) XRD pattern of N-Ru/C. # represents the peak of carbon. (b, c) Ru 3p and N 1 s core-level XPS spectra of N-Ru/C and Ru/C catalysts, respectively. (d, e) TEM images of N-Ru/C catalyst. (f) HAADF-STEM images and EDX elemental mapping of Ru and N in N-Ru/C.

toward HOR and HER in alkaline media. The X-ray photoelectron spectroscopy (XPS) and density functional theory (DFT) calculation results indicated the electron transfer between Ru and N. We further found that the introduction of N could weaken the H binding strength of Ru to become much closer to zero and consequently boost the HOR/HER performance.

The Ru nanoparticles (NPs) were first synthesized using a simple colloidal method. Dodecylamine (DDA) and oleic acid (OA) were used as the solvent. $RuCl_3 \cdot nH_2O$ was used as Ru precursor. The N-Ru/C was obtained by annealing the as-prepared Ru nanoparticles supported on XC-72 carbon at 400 °C under NH_3 atmosphere. The different contents of nitrogen element in Ru nanoparticles were obtained by controlling different annealing time for 10, 30 and 60 min, denoted as N-Ru-1/C, N-Ru-2/C and N-Ru-3/C, respectively. The different N contents were listed in Table S1 (Supporting information) conducted by X-ray photoelectron spectroscopy (XPS). It is obvious that the N content is increased with the reaction time. Because of the highest catalytic HOR/HER activities of N-Ru-2/C, N-Ru/C in the whole text represented N-Ru-2/C (*vide infra*). The structure of N-Ru/C was firstly characterized by powder X-ray diffraction (XRD). The diffraction peaks of N-Ru/C shown in Fig. 1a can be well attributed to metallic Ru in hexagonal phase (JCPDS No. 06-0663), which is similar with that of Ru/C with no obvious change of the crystal structure (Fig. S1 in Supporting information). For comparison, the XRD patterns of N-Ru-1/C and N-Ru-3/C are shown in Figs. S2 and S3 (Supporting information). All the diffraction peaks of these catalysts are well-assigned to hexagonal Ru. The XPS spectra of N-Ru/C and Ru/C in the Ru 3p regions were shown in Fig. 1b. Both two characteristic peaks corresponding to Ru $3p_{3/2}$ and $3p_{1/2}$ are observed. Notably, the binding energy of the Ru $3p_{3/2}$ characteristic peak (461.8 eV) in N-Ru/C is slightly shifted to higher position compared to that in Ru/C (461.4 eV), suggesting N gains electrons from Ru in N-Ru/C. Fig. 1c shows the high-resolution XPS spectra of N 1s of N-Ru/C, which further indicates the presence of nitrogen. The XPS survey and XPS data of C in N-Ru/C are shown in Figs. S4 and S5 (Supporting information).

The morphology of N-Ru/C was investigated by transmission electron microscopy (TEM). As shown in Fig. 1d, the N-Ru NPs are well-dispersed on the XC-72 carbon support with the average particle size of about 3.1 nm (Fig. S6 in Supporting information). Fig. 1e displays the high-resolution TEM image of N-Ru/C and an interplanar spacing of about 0.207 nm can be observed, which is assigned to the (101) plane of the hexagonal Ru structure. In addition, to further identify the structure of the N-Ru/C, the high-angle annular dark field scanning TEM image (HAADF-STEM) and energy-dispersive spectroscopy (EDS) mapping were conducted. Fig. 1f indicates that the Ru and N atoms are uniformly distributed on the N-Ru NPs. Furthermore, the TEM images and size distributions of N-Ru-1/C, N-Ru-3/C, and Ru/C are displayed in Figs. S7-S9 (Supporting information). All of these N-Ru or Ru NPs are well-dispersed on the XC-72 carbon support with the average particle sizes of about 3.1, 3.3 and 3.6 nm for N-Ru-1/C, N-Ru-3/C and Ru/C, respectively.

The HOR performances of the different N-Ru/C catalysts were first evaluated in 0.1 mol/L KOH. The loading of the platinum group metal (PGM) in all the as-prepared catalysts were gained by inductively coupled plasma-atomic emission spectroscopy (ICP-AES) (Table S2 in Supporting information). The cyclic voltammetry (CV) curves (Fig. S10a in Supporting information) of all the N-Ru/C catalysts show that HOR current densities firstly increase up to around 0.1 V and then decrease because of the Ru surface oxidation and the desorption of underpotentially deposited hydrogen (H-UPD) [41-44]. Similar phenomena can be seen in the polarization curves (Fig. S10b in Supporting information). After the linear fitting of micro-polarization region (−5~5 mV) by the approximate Butler-Volmer equation (Fig. S10c in Supporting information) [5,41], exchange current densities (j^0) of the N-Ru/C catalysts are obtained. As can be seen, the N-Ru-2/C has the maximal slope among all the N-Ru/C catalysts, indicating its best apparent activity. The mass-specific exchange current density ($j^{0,m}$), also called mass activity (MA), is obtained after j^0 being normalized by the loading of the PGM. Furthermore, Cu underpotential deposition (Cu-UPD) stripping strategy is used to evaluate the electrochemically active surface area (ECSA) of different catalysts and further clarify the electrocatalytic active sites (Fig. S11 and Table S3 in Supporting information) [41]. The area-specific exchange current density ($j^{0,s}$), also named specific activity (SA), is calculated after j^0 being normalized by the ECSAs of these catalysts. The final $j^{0,m}$ and $j^{0,s}$ of different N-Ru/C catalysts are displayed in Table S3 and Fig. S10d (Supporting information). The $j^{0,m}$ of N-Ru-1/C, N-Ru-2/C and N-Ru-3/C are calculated to be 0.21, 0.54 and 0.34 mA/μg, respectively. The $j^{0,s}$ of N-Ru-1/C, N-Ru-2/C and N-Ru-3/C are calculated to be 0.23, 0.56 and 0.37 mA/cm^2, respectively.

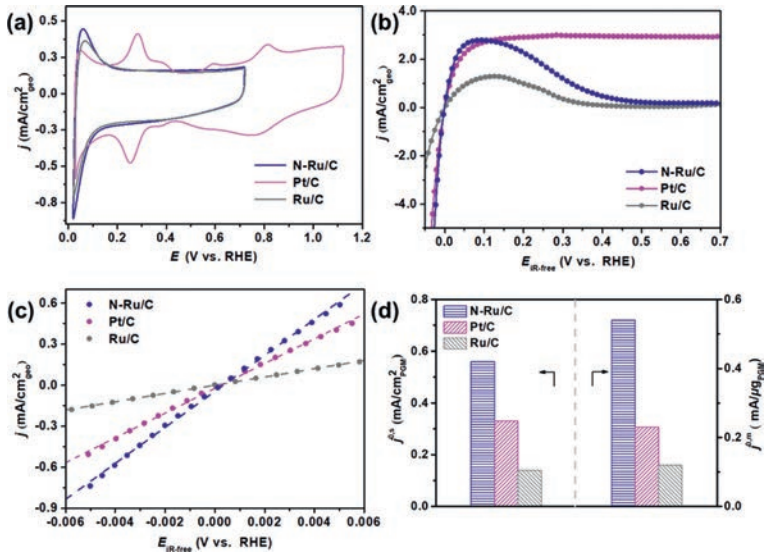

Fig. 2. (a) CVs curves of N-Ru/C, Pt/C and Ru/C conducted in Ar-saturated 0.1 mol/L KOH at a scan rate of 50 mV/s. (b) HOR polarization curves and (c) linear-current potential region around the equilibrium potential of HOR/HER of N-Ru/C, Pt/C and Ru/C conducted in H_2-saturated 0.1 mol/L KOH at a scan rate of 10 mV/s with the rotation speed at 1600 rpm after *i*R-compensation. (d) MA and SA of N-Ru/C, Pt/C and Ru/C in 0.1 mol/L KOH.

The N-Ru-2/C possesses the highest mass activity and specific activity.

Furthermore, the HOR performances of N-Ru/C, Ru/C, and Pt/C (20 wt%) were also explored. Their CV curves obtained in Ar-saturated KOH and polarization curves obtained in H_2-saturated KOH were shown in Fig. 2a and b. For both N-Ru/C and Ru/C, the peaks at around 0.1 V attributed to the Ru surface oxidation and H-UPD can be clearly observed. After the linear fitting of micro-polarization region (−5~5 mV) by the approximate Butler-Volmer equation (Fig. 2c), j^0 of the N-Ru/C, Ru/C and Pt/C are obtained. As can be seen, the N-Ru/C has the maximal slope among all the three catalysts, indicating its best apparent activity. After normalizing the j^0 of N-Ru/C, Ru/C and Pt/C by the loading of the PGM (Table S2) and the ECSAs (Figs. S11 and S12 in Supporting information), the obtained $j^{0,m}$ of N-Ru/C, Ru/C, and Pt/C are calculated to be 0.54, 0.12 and 0.23 mA/μg, respectively (Fig. 2d and Table S3). And the $j^{0,s}$ of N-Ru/C, Ru/C and Pt/C are calculated to be 0.56, 0.14 and 0.33 mA/cm^2, respectively (Fig. 2d and Table S3). The above results indicate the N-Ru/C display excellent mass activity and specific activity. The MA of N-Ru/C is about 4.5 and 2 times higher than that of Ru/C and Pt/C, respectively. The SA of N-Ru/C is about 4 and 2 times higher than that of Ru/C and Pt/C, respectively. Notably, the $j^{0,m}$ and $j^{0,s}$ of N-Ru/C surpass most of the reported PGM-based catalysts (Table S4 in Supporting information). However, though N-Ru/C exhibits excellent HOR activity, the drawback of Ru-based electrocatalyst is that Ru is easily oxidized. The generated oxygenated species on the catalyst surface will inhibit H_2 adsorption, and consequently, the HOR current will decrease around 0.1~0.2 V [21,41-44]. To date, no rational approach has been proposed to circumvent the electrochemical oxidation of the Ru surface. Therefore, further research is needed in the future.

Stability is another important factor to evaluate a catalyst. Hence, the stability N-Ru/C was carried out using accelerated durability tests (ADTs) (Fig. S13 in Supporting information). The CV and polarization curves before and after 1000 CVs show almost no variation (Figs. S13a and b). The j^0 calculated from micro-polarization region of N-Ru-2/C (Fig. S13c) exhibits a decreasing tendency from 2.65 mA/cm^2 to 2.52 mA/cm^2, suffering a loss of 5% in HOR activity (Fig. S13d), suggesting the good stability of N-Ru/C in alkaline media. The chronoamperometry was further conducted to test the stability of N-Ru/C (Fig. S14 in Supporting information). After 20000s, the N-Ru/C only shows a small decay in current density. Furthermore, there are no obvious changes in TEM, XRD and XPS of N-Ru/C carried out after ADTs (Fig. S15 in Supporting information) compared with those before ADTs. These results also suggest the good durability of N-Ru/C toward alkaline HOR.

The electrocatalytic HER activities of all the N-Ru/C catalysts were also explored in order to investigate the impact on HER activity of different N contents in 1.0 mol/L KOH solution. Fig. S16a shows their HER polarization curves. The overpotentials to achieve 10 mA/cm^2 (η_{10}) of N-Ru-1/C, N-Ru-2/C and N-Ru-3/C are 67, 31 and 46 mV, respectively. Fig. S16b (Supporting information) shows their relevant Tafel plots. The Tafel slopes of N-Ru-1/C, N-Ru-2/C and N-Ru-3/C are 125, 106 and 118 mV/dec, respectively. These results indicate that N-Ru-2/C has the highest HER activity and the fastest reaction kinetics among all the N-Ru/C catalysts. Fig. S16c (Supporting information) displays their corresponding polarization curves normalized by the loading of the PGM, exhibiting the same tendency of HER polarization curves. Fig. S16d (Supporting information) also exhibits that N-Ru-2/C possesses the highest mass activity.

The HER performances of N-Ru/C, Ru/C and Pt/C (20 wt%) were further conducted for better comparison. The η_{10} of N-Ru/C, Ru/C and Pt/C are 31, 106 and 43 mV, respectively (Fig. 3a). Notably, the η_{10} of N-Ru/C surpass most of the reported electrocatalysts (Table S5 in Supporting information). The Tafel slopes of N-Ru/C, Ru/C and Pt/C are 106, 131 and 110 mV/dec, respectively (Fig. 3b). After normalized with the loading of the PGM, the HER polarization curves of these three catalysts in Fig. 3c shows the same tendency. The obtained current density (j_m) at overpotential varying form 10 mV to 50 mV are presented in Fig. 3d. It is obvious to see that N-Ru/C possesses higher current density at the same overpotential compared to Ru/C and Pt/C. The j_m of N-Ru/C is 0.90 mA/μg at η = 50 mV, which is about 5.5 and 2 times higher than that of Ru/C (0.16 mA/μg) and Pt/C (0.45 mA/μg). In addition, the stability of the N-Ru/C was also carried out. After 1000 CVs, the HER polarization curve of N-Ru/C is almost the same with that before 1000 CVs (Fig. S17a in Supporting information). In addition, there is no obvious change in overpotential during the long-time chronopotentiometry test (Fig. S17b in Supporting information). Furthermore, XRD, TEM and XPS of N-Ru/C after the stability test (Fig. S18 in

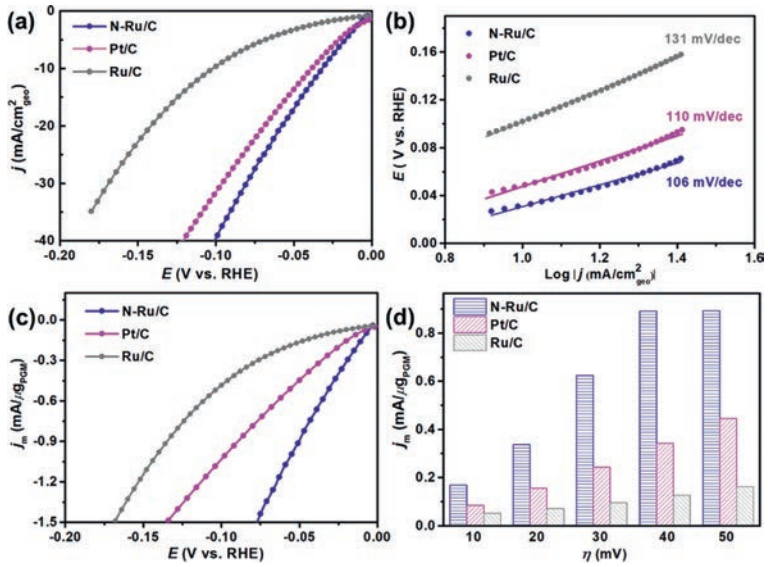

Fig. 3. (a) HER polarization curves of N-Ru/C, Pt/C and Ru/C in 1.0 mol/L KOH. (b) The corresponding Tafel plots. (c, d) HER polarization curves and the corresponding exchange current density at different overpotentials of N-Ru/C, Pt/C and Ru/C in 1.0 mol/L KOH normalized with the loading of PGM calculated by ICP-AES (Table S2).

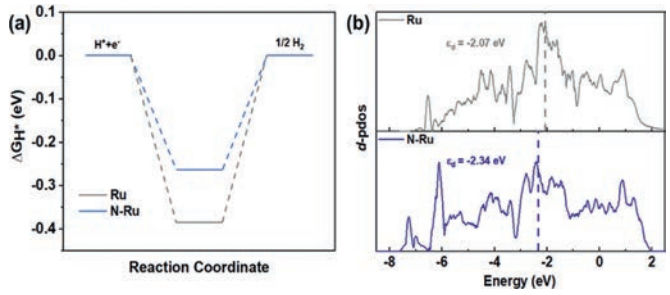

Fig. 4. (a) The hydrogen adsorption free energy (ΔG_{H^*}) on Ru and N-Ru. (b) The *d*-pdos of Ru of pure Ru and N-Ru.

Supporting information) show no apparent changes compared with those of N-Ru/C before the stability test, indicating its good HER stability in alkaline solution.

To further understand the origin of enhanced alkaline HOR/HER activity of N-Ru/C, density functional theory (DFT) calculations were conducted. On the basis of the Volcano plot, the HOR/HER activity of a catalyst depends on its value of hydrogen adsorption Gibbs free energy (ΔG_{H^*}) [45,46]. And the ΔG_{H^*} value of a good electrocatalyst should be close to zero, which means suitable H chemisorption and releasing strength. Therefore, we calculated the ΔG_{H^*} on Ru (001) surface with and without N doping. The theoretical structures of Ru and N-Ru before and after the adsorption of H were shown in Fig. S19 (Supporting information). As shown in Fig. 4a, the calculated values of ΔG_{H^*} on Ru and N-Ru models are −0.39 eV and −0.29 eV, respectively, revealing that the doping of N weaken the binding energy of Ru with hydrogen. The *d*-band center (ε_d) theory developed by Nørskov *et al*. states that metals with the ε_d closer to the Fermi level are more active than those with the ε_d further away from the Fermi level, which means the lower ε_d could give rise to weaker binding strength between adsorbates and catalysts [47,48]. Thus, the *d*-orbital partial density of states (*d*-pdos) of Ru and N-Ru were calculated. The downshift trend of the *d*-band centers from Ru (−2.07 eV) to N-Ru (−2.34 eV) corresponding to the weaker H binding strength of N-Ru (Fig. 4b). The Bader charges of Ru atoms and N atoms (Fig. S20 in Supporting information) were also calculated and shown in Table S6 (Supporting information), and the results indicate that partial electrons transfer from Ru to N, which is consistent with the XPS analysis. Thus, the incorporation of N could regulate the electronic structure of Ru, thereby weaken H binding strength of Ru to become closer to zero and consequently enhance the HOR/HER activity.

In summary, we have developed an efficient strategy to boost the HOR/HER performance of Ru through N-incorporation. As expected, the resulted N-Ru/C catalysts exhibit remarkable HOR/HER performance under alkaline media, with the HOR activity 4.5 and 4 times higher than Ru/C in terms of both MA and SA, and even surpassing the commercial Pt/C. In addition, at the overpotential of 50 mV, the normalized HER current density of N-Ru/C is 5.5 times higher than that of Ru/C. Experimental and density functional theory (DFT) calculation results indicate that the enhanced HOR/HER performances are derived from optimized hydrogen adsorption Gibbs free energy (ΔG_{H^*}) of N-Ru/C after N incorporation. This study provides a new way for the rational design of Pt-free catalysts for catalyzing alkaline HOR/HER.

Declaration of competing interest

The authors declare that they have no known competing financial interests or personal relationships that could have appeared to influence the work reported in this paper.

Acknowledgments

This work was financially supported by the National Natural Science Foundation of China (No. 21972107), National Natural Science Foundation of Hubei Province (No. 2020CFA095), the National Natural Science Foundation of Jiangsu Province (No. BK20191186) and Yangzhou Key Research Development Program (No. YZ2019025). The numerical calculations in this paper have been done on the supercomputing system in the Supercomputing Center of Wuhan University.

Supplementary materials

Supplementary material associated with this article can be found, in the online version, at doi:10.1016/j.cclet.2021.05.038.

References

[1] J.A. Turner, Science 305 (2004) 972–974.
[2] I. Staffell, D. Scamman, A. Velazquez Abad, et al., Energy Environ. Sci. 12 (2019) 463–491.
[3] F. Dawood, M. Anda, G.M. Shafiullah, Int. J. Hydrogen Energy 45 (2020) 3847–3869.
[4] Y. Mena, J. Sub, X. Wang, et al., Chin. Chem. Lett. 30 (2019) 634–637.
[5] S. Lu, Z. Zhuang, Sci. China Mater. 59 (2016) 217–238.
[6] X. Tian, P. Zhao, W. Sheng, Adv. Mater. 31 (2019) e1808066.
[7] C. Hu, L. Zhang, J. Gong, Energy Environ. Sci. 12 (2019) 2620–2645.
[8] X. Ge, A. Sumboja, D. Wuu, et al., ACS Catal. 5 (2015) 4643–4667.
[9] J.R. Varcoe, P. Atanassov, D.R. Dekel, et al., Energy Environ. Sci. 7 (2014) 3135–3191.
[10] J. Durst, A. Siebel, C. Simon, et al., Energy Environ. Sci. 7 (2014) 2255–2260.
[11] W. Sheng, H.A. Gasteiger, Y. Shao-Horn, J. Electrochem. Soc 157 (2010) B1529–B1536.
[12] Y. Deng, L. Yang, Y. Wang, et al., Chin. Chem. Lett. 32 (2021) 511–515.
[13] J. Yu, Q. He, G. Yang, et al., ACS Catal. 9 (2019) 9973–10011.
[14] S. Han, Q. Yun, S. Tu, et al., J. Mater. Chem. A 7 (2019) 24691–24714.
[15] C. Li, J.B. Baek, ACS Omega 5 (2020) 31–40.
[16] W. Luo, Y. Wang, C. Cheng, Mater. Today Phys. 15 (2020) 100274.
[17] Y. Zhao, H. Cong, P. Li, et al., Angew. Chem. Int. Ed. 60 (2021) 7013–7017.
[18] S. Zhang, J. Li, E. Wang, ChemElectroChem 7 (2020) 4526–4534.
[19] Y. Li, J. Abbott, Y. Sun, et al., Appl. Catal. B: Environ. 258 (2019) 117952 117952.
[20] Y. Cong, B. Yi, Y. Song, Nano Energy 44 (2018) 288–303.
[21] E.S. Davydova, S. Mukerjee, F. Jaouen, et al., ACS Catal 8 (2018) 6665–6690.
[22] J. Zhu, L. Hu, P. Zhao, et al., Chem. Rev. 120 (2020) 851–918.
[23] B. Wang, X. Cui, J. Huang, et al., Chin. Chem. Lett. 29 (2018) 1757–1767.
[24] L. Fu, Y. Li, N. Yao, et al., ACS Catal. 10 (2020) 7322–7327.
[25] L. Fu, F. Yang, Y. Hu, et al., Sci. Bull. 65 (2020) 1735–1742.
[26] J. Song, Y.Q. Jin, L. Zhang, et al., Adv. Energy Mater. 11 (2021) 2003511.
[27] J.A. Bau, S.M. Kozlov, L.M. Azofra, et al., ACS Catal. 10 (2020) 12858–12866.
[28] F. Yang, X. Bao, P. Li, et al., Angew. Chem. Int. Ed. 58 (2019) 14179–14183.
[29] N. Yao, R. Meng, F. Wu, et al., Appl. Catal. B-Environ. 277 (2020) 119282.
[30] A.R. Puente Santiago, T. He, O. Eraso, et al., J. Am. Chem. Soc. 142 (2020) 17923–17927.
[31] F. Yang, P. Han, N. Yao, et al., Chem. Sci. 11 (2020) 12118–12123.
[32] W. Li, Y. Zhao, Y. Liu, et al., Angew. Chem. Int. Ed. 60 (2021) 3290–3298.
[33] X. Wang, Y. Zhu, A. Vasileff, et al., ACS Energy Lett. 3 (2018) 1198–1204.
[34] S.C. Sarma, V. Mishra, K.A. Ann Mary, et al., ACS Energy Lett. 3 (2018) 3008–3014.
[35] K. Chen, S. Deng, Y. Lu, et al., Chin. Chem. Lett. 32 (2021) 765–769.
[36] E. Cao, Z. Chen, H. Wu, et al., Angew. Chem. Int. Ed. 59 (2020) 4154–4160.
[37] Y. Zhao, X. Wang, G. Cheng, et al., ACS Catal. 10 (2020) 11751–11757.
[38] Y. Men, Y. Tan, P. Li, et al., Appl. Catal. B: Environ. 284 (2021) 119718.
[39] N. Yao, P. Li, Z. Zhou, et al., Adv. Energy Mater. 9 (2019) 1902449.
[40] Y. Wei, X. Zhang, Z. Wang, et al., Chin. Chem. Lett. 32 (2021) 119–124.
[41] J. Ohyama, T. Sato, Y. Yamamoto, et al., J. Am. Chem. Soc. 135 (2013) 8016–8021.
[42] S. Hadzi-Jordanov, H. Angerstein-Kozlowska, M. Vukovic, et al., J. Phys. Chem. 81 (1977) 2271–2279.
[43] H. Inoue, J.X. Wang, K. Sasaki, et al., J. Electroanal. Chem 554-555 (2003) 77–85.
[44] H.A. Gasteiger, N.M. Markovic, P.N. Ross, J. Phys. Chem. 99 (1995) 8290–8301.
[45] W. Sheng, M. Myint, J.G. Chen, et al., Energy Environ. Sci. 6 (2013) 1509–1512.
[46] J.K. Nørskov, T. Bligaard, A. Logadottir, et al., J. Electrochem. Soc. 152 (2005) J23–J26.
[47] B. Hammer, O.H. Nielsen, J.K. Nrskov, Catal. Lett. 46 (1997) 31–35.
[48] B. Hammer, J.K Norskov, Nature 376 (1995) 238–240.